Journal Name

ARTICLE TYPE

Cite this: DOI: 10.1039/xxxxxxxxxx

Supplementary Material: Disentangling defects and sound modes in disordered solids

Sven Wijtmans,[a] and M. Lisa Manning[b]

Received Date
Accepted Date

DOI: 10.1039/xxxxxxxxxx

www.rsc.org/journalname

Section I: Derivation of the augmented potential

In this section, we derive the augmented dynamical matrix that allows us to separate localized modes from extended plane-wave-like modes at low frequency in a disordered solid. Latin indices are used to label particles and greek indices to label cartesian components. All summations are explicit.

The low frequency vibrational modes of a disordered solid contain localized excitations at defects hybridized with extended plane-wave-like modes and are the eigenvectors of the Dynamical matrix $M_{i\alpha j\beta} = \frac{\partial^2 U}{\partial u_{i\alpha}\partial u_{j\beta}}$. In order to examine the bare defects, we must separate these two types of modes. To prevent hybridization, our goal is to increase the energy of the plane-wave-like modes without increasing the energy of the localized modes.

To do this, we add an extra term to the total energy of the packing U that represents a grid of virtual points connected by a spring-like interaction. The motion of each grid point is defined as the motion of the particles near it, weighted by a Gaussian function of the distance between them. The new energy is then

$$\tilde{U} = \frac{1}{2}\left(\sum_{i}^{n}\sum_{j}^{n}\sum_{\alpha}^{x,y}\sum_{\beta}^{x,y} u_{i\alpha}M_{i\alpha j\beta}u_{j\beta} + \sum_{k}^{g^2}\sum_{l}^{g^2}\sum_{\gamma}^{x,y} K_{kl}\left(\tilde{u}_{k\gamma} - \tilde{u}_{l\gamma}\right)^2\right), \quad (1)$$

where

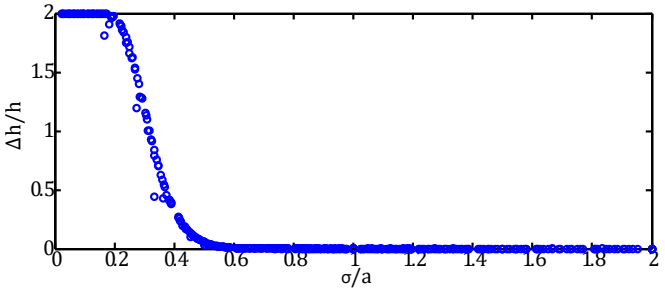

Fig. 1 Ratio of height variation Δh to mean height $\bar{h}$ of a grid of gaussians of width σ and spacing a between each peak.

$$\tilde{u}_{k\gamma} = \frac{\sum_{p}^{n} u_{p\gamma}\mathrm{Exp}\left[-\sum_{\eta}^{x,y}\left(x_{p\eta} - k_\eta a\right)^2/\sigma^2\right]}{\sum_{p}^{n}\mathrm{Exp}\left[-\sum_{\eta}^{x,y}\left(x_{p\eta} - k_\eta a\right)^2/\sigma^2\right]}, \quad (2)$$

$$k_x = \mathrm{Floor}[k/g], \quad (3)$$

$$k_y = \mathrm{Mod}[k, g], \quad (4)$$

$$g = L/a, \quad (5)$$

where g is the number of grid points per side, a is the spacing between grid points, and L is the side length. K_{kl} sets the connectivity and the strength of the connection between grid points. In this work, we connect adjacent grid points on a square grid, so that $K_{kl} = K\delta_{k,l\pm1}$.

The width of the Gaussian weighting is set equal to the grid spacing, as the sum of a grid of Gaussians with width equal to the spacing is flat to within 10^{-6}, as seen in Fig.1. We divide by the Gaussian contribution of each particle near the grid point to normalize by particle density.

The total augmented energy can be written as a quadratic function in terms of the standard dynamical matrix M and the dynamical matrix $M^\dagger$ corresponding to the augmented potential:

[a] Syracuse University, Syracuse, New York 13244, USA E-mail: sfwijtma@syr.edu
[b] Syracuse University, Syracuse, New York 13244, USA E-mail: mmanning@syr.edu

$$\tilde{U} = \frac{1}{2}\left(\sum_{i}^{n}\sum_{j}^{n}\sum_{\alpha}^{x,y}\sum_{\beta}^{x,y} u_{i\alpha}\left(M_{i\alpha j\beta} + M^{\dagger}_{i\alpha j\beta}\right)u_{j\beta}\right). \quad (6)$$

To simplify notation, we introduce a weighing function

$$W(i,l) = \frac{\mathrm{Exp}\left[-\sum_{\eta}^{x,y}\left(x_{i\eta} - l_{\eta}a\right)^2/\sigma^2\right]}{\sum_{p}^{n}\mathrm{Exp}\left[-\sum_{\eta}^{x,y}\left(x_{i\eta} - l_{\eta}a\right)^2/\sigma^2\right]}. \quad (7)$$

and then $\tilde{U}$ becomes:

$$\tilde{U} = \frac{1}{2}\left(\sum_{i}^{n}\sum_{j}^{n}\sum_{\alpha}^{x,y}\sum_{\beta}^{x,y} u_{i\alpha}M_{i\alpha j\beta}u_{j\beta} + \sum_{k}^{g^2}\sum_{l}^{g^2}\sum_{\gamma}^{x,y} K_{kl}\left(\left(\sum_{p}^{n}u_{p\gamma}W(p,k)\right)\left(\sum_{p}^{n}u_{p\gamma}W(p,k)\right) - 2\left(\sum_{p}^{n}u_{p\gamma}W(p,k)\right)\left(\sum_{p}^{n}u_{p\gamma}W(p,l)\right) + \left(\sum_{p}^{n}u_{p\gamma}W(p,l)\right)\left(\sum_{p}^{n}u_{p\gamma}W(p,l)\right)\right)\right). \quad (8)$$

Without loss of generality, we reindex the summations from p to i and j

$$\tilde{U} = \frac{1}{2}\left(\sum_{i}^{n}\sum_{j}^{n}\sum_{\alpha}^{x,y}\sum_{\beta}^{x,y} u_{i\alpha}M_{i\alpha j\beta}u_{j\beta} + \sum_{k}^{g^2}\sum_{l}^{g^2}\sum_{\gamma}^{x,y} K_{kl}\left(\left(\sum_{i}^{n}u_{i\gamma}W(i,k)\right)\left(\sum_{j}^{n}u_{j\gamma}W(j,k)\right) - 2\left(\sum_{i}^{n}u_{i\gamma}W(i,k)\right)\left(\sum_{j}^{n}u_{j\gamma}W(j,l)\right) + \left(\sum_{i}^{n}u_{i\gamma}W(i,l)\right)\left(\sum_{j}^{n}u_{j\gamma}W(j,l)\right)\right)\right). \quad (9)$$

As each term has a sum over i and j, these can be grouped

$$\tilde{U} = \frac{1}{2}\sum_{i}^{n}\sum_{j}^{n}\left(\sum_{\alpha}^{x,y}\sum_{\beta}^{x,y} u_{i\alpha}M_{i\alpha j\beta}u_{j\beta} + \sum_{k}^{g^2}\sum_{l}^{g^2}\sum_{\gamma}^{x,y} K_{kl}u_{i\gamma}u_{j\gamma}\Big(W(i,k)W(j,k) - 2W(i,k)W(j,l) + W(i,l)W(j,l)\Big)\right). \quad (10)$$

We reindex again:

$$\sum_{\gamma} u_{i\gamma}u_{j\gamma} = \sum_{\alpha} u_{i\alpha}u_{j\alpha}, \quad (11)$$

$$\sum_{\alpha} u_{i\alpha}u_{j\alpha} = \sum_{\alpha}\sum_{\beta} u_{i\alpha}u_{j\beta}\delta_{\alpha\beta}, \quad (12)$$

by definition of Kronecker delta. Grouping the dimension sums and gathering terms we find

$$\tilde{U} = \frac{1}{2}\sum_{i}^{n}\sum_{j}^{n}\sum_{\alpha}^{x,y}\sum_{\beta}^{x,y}\left(u_{i\alpha}\left(M_{i\alpha j\beta} + \delta_{\alpha\beta}\sum_{k}^{g^2}\sum_{l}^{g^2}K_{kl}\Big(W(i,k)*W(j,k) - 2W(i,k)*W(j,l) + W(i,l)*W(j,l)\Big)\right)u_{j\beta}\right) \quad (13)$$

,

resulting in the final definition of $M^{\dagger}$,

$$M^{\dagger} = \sum_{k}^{g^2}\sum_{l}^{g^2}K_{kl}\delta_{\alpha\beta}\big(W(i,k)W(j,k) - 2W(i,k)W(j,l) + W(i,l)W(j,l)\big). \quad (14)$$

We can analytically determine the energy increase for plane waves by assuming a continuous field of particles, which allows us to go from a summation to an integral over particle positions. We let the plane wave be defined as

$$u_x = A\sin(2\pi kx/L + \phi), u_y = 0. \quad (15)$$

Then the continuous form is

$$U^{\dagger} = \sum_{k_x=1}^{Gt}\sum_{l_x=1}^{Gt}\sum_{k_y=1}^{Gt}\sum_{l_y=1}^{Gt}\left(\delta(l_x,k_x\pm 1)\delta(l_y,k_y\pm 1)K \int_{-\infty}^{\infty}\int_{-\infty}^{\infty}\left(dxdy\frac{A}{\pi\sigma^2}\sin(2\pi kx/L+\phi)\left(e^{-\frac{(x-ak_x)^2+(y-ak_y)^2}{\sigma^2}} - e^{-\frac{(x-al_x)^2+(y-al_y)^2}{\sigma^2}}\right)\right)\right). \quad (16)$$

In order to deal with boundary conditions, we take the limit as $Gt \to \infty$. we also set $\sigma = a$, and $\lambda = L/k$. This computation gives the result

$$U^{\dagger} = -4\pi^2A^2Ke^{-\frac{8\pi^4a^2}{\lambda^2}}\left(\cos\left(\frac{4\pi^2a}{\lambda}\right) - 1\right). \quad (17)$$

which is shown by the dashed lines in Fig. 2 in the main text.

Section II: Choosing model parameters

To choose a value for the parameter K, the connection strength, we calculate the total number of localized modes of the 50 low-

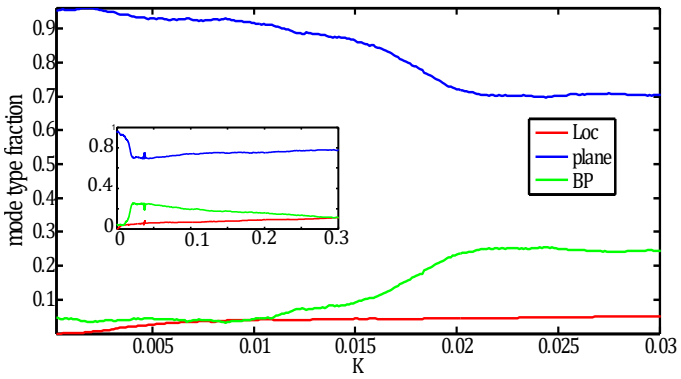

Fig. 2 The 50 lowest frequency modes in 100 packings, sorted by type as in Fig.3 b, plotted as a function of K. There are three regions: $0 < K < 0.01$, where the augmentation begins to have an effect, $0.01 < K < 0.02$, where the augmentation begins to greatly alter the mode structure, and $0.02 < K$, where the number of spurious localized modes grow linearly with K, as shown in the inset over a wider range of K.

est frequency modes in the packing as a function of K, where localized modes are defined using the radius of gyration as defined in the main text. As seen in Fig 2, the number of localized modes grows until a value of $K = 0.01$, and essentially plateaus thereafter. Additionally, the number of boson peak modes is relatively constant until the same value. Furthermore, the number of plane-wave modes begins a more sharp decline at that value. Taken together, this suggests that a value of $K = 0.01$ balances the augmented energy with the internal potential energy to shift plane waves without generating spurious localized modes.

Section III: Defining a new state

In order to define a new state, we examine seven independent criteria: i) any change in the contact network (CR+), ii) non-rattler[1] contact changes (CR-), iii) requiring more than two particles to change contacts (C2), iv) energy differences between the original and final basins of greater than 10^{-8} (E-8), v) a displacement of a single particle more than two large particle diameters in a direction perpendicular to the mode (D), vi) having a significant stress drop (S), and vii) requiring that more than 2 contact changing particles must be neighbors, thereby rearranging as a unit, (C2N).

As shown in Fig. 3, for each standard mode and each of the first five definitions, we measure the ratio between the energy barrier calculated using that definition and C2N ($\Delta U/\Delta U^{C2N}$).Several of these criteria, such as contact changes that include or exclude rattlers (CR+, CR-), generate energy barriers that are significantly lower than the other criteria and different from each other. We note that these definitions have been used for studies of energy barriers in the past[2]. This result suggests that these criteria generate a lot of "false positives" – they identify changes to the network that do not correspond to a particle rearrangement. In contrast, the four other methods (C2, E-8, D, S) generate distributions of energy barriers with the same median as C2N, indicating that these criteria are very similar and likely identify particle rearrangements associated with saddle points and plasticity.

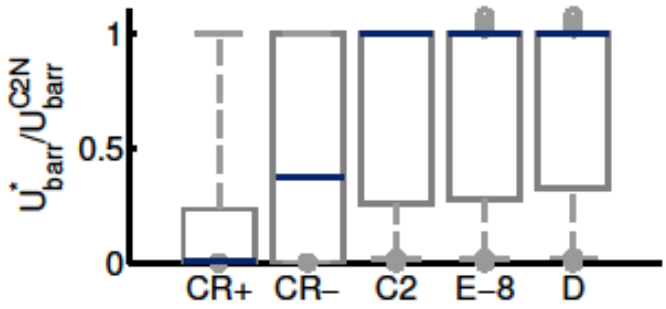

Fig. 3 Ratio of energy barriers $\Delta U/\Delta U^{C2N}$ calculated using different definitions for what constitutes a particle rearrangement, as described in the main text. Box and whiskers contains 50 % and 92 % of the data points, respectively, blue bars denote the median, and outliers are circles.

Section IV: Defect size and predictive capability

As discussed in the main text, we find that the augmented modes are just as predictive as standard modes if we use the soft spot algorithm to correlate localized excitations with plasticity, and we can use fewer modes (15 augmented modes compared to 25 standard modes).

As a third measure of whether localized excitations predict plastic events, we compare the distance between the center of mass of the localized excitation and the center of mass of the rearrangement.

Of course, we expect that this distance will scale with the number density of candidate defects, so we first calculate the probability density P for the minimum distance r between the origin and n points randomly distributed in 2D space:

$$P(r,n) = 2\pi n r\Theta\left(\frac{1}{2}-r\right)\left(1-\pi r^2\right)^{n-1} - n\Theta\left(r-\frac{1}{2}\right) * \left(-\frac{4r}{\sqrt{4r^2-1}} + \frac{4}{\sqrt{4-\frac{1}{r^2}}} + 2r\left(\pi - 4\csc^{-1}(2r)\right)\right) * \left(-\sqrt{4r^2-1} + r^2\left(\pi - 4\csc^{-1}(2r)\right)+1\right)^{n-1}, \quad (18)$$

where Θ is the Heavyside function. The expected minimum distance for n randomly distributed points is then $d^n_{rand} = \int rP(r,n)dr$.

Given the location of the center of a rearrangement and a list of n locations corresponding to centers of localized excitations, we compute the minimum distance between the rearrangement and any localized excitation d^n. We then normalize d^n by the value of a random distribution, d^n_{rand}, and if our rearrangements are predictive then $d \equiv d^n/d^n_{rand} < 1$, and there is no bias as a function of the number or size of the localized regions.

We compare the distributions of d for several different definitions of localized excitations. We first assume every localized augmented mode corresponds to a defect, and compare d just before (at a strain 10^{-6} below the critical strain) the event (denoted 'near'), as well as immediately after the previous rearrangement

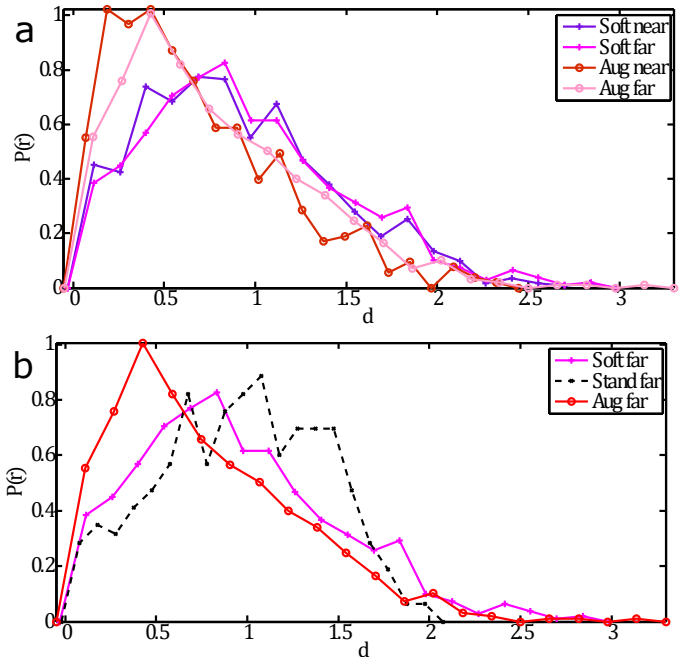

Fig. 4 Comparison of the separation distances between the center of a mode and the center of a rearrangement. We compare standard modes, augmented modes, and soft spots, near and far from the rearrangement, as well as a comparison to a random distribution of the same number as described in Section III. Each line is scaled by the expected value of a random distribution of the same number of candidates.

(far). We repeat this procedure for the standard modes and soft spots generated by the method of Manning and Liu[3].

As shown in Fig. 4, using this strict metric, the augmented modes display significant improvement over a random distribution with the same number of candidates (e.g. $\langle d \rangle < 1$). The augmented modes are also closer in distance to the rearrangement than soft spots once controlled for the number of candidates.

As discussed in the main text, we also want to understand how the size of localized augmented excitations compares to the size of soft spots. To this end, we use the published soft spots algorithm to identify the optimal number of modes ($N_m = 25$) and number of particles ($N_p = 20$). A histogram for the number of spots and their size are shown by the black data points in Fig. 5 a and b, respectively. Next, we only study soft spots generated from localized augmented modes, and since there are only ~ 7 such modes we expect to find approximately that number of soft spots, which is the case, as shown by the red and magenta data points in Fig 5a. The correlation with rearrangements is largely insensitive to N_p for values between 20 and 30, but N_p does affect soft spot size, as shown in Fig. 5b.

References

1 A rattler is defined as any particle with less than three contacts.

2 N. Xu, V. Vitelli, A. J. Liu and S. R. Nagel, *EPL (Europhysics Letters)*, 2009, **90**, 6.

3 M. L. Manning, J. S. Langer and J. M. Carlson, *Physical Review E - Statistical, Nonlinear, and Soft Matter Physics*, 2007, **76**, 056106.

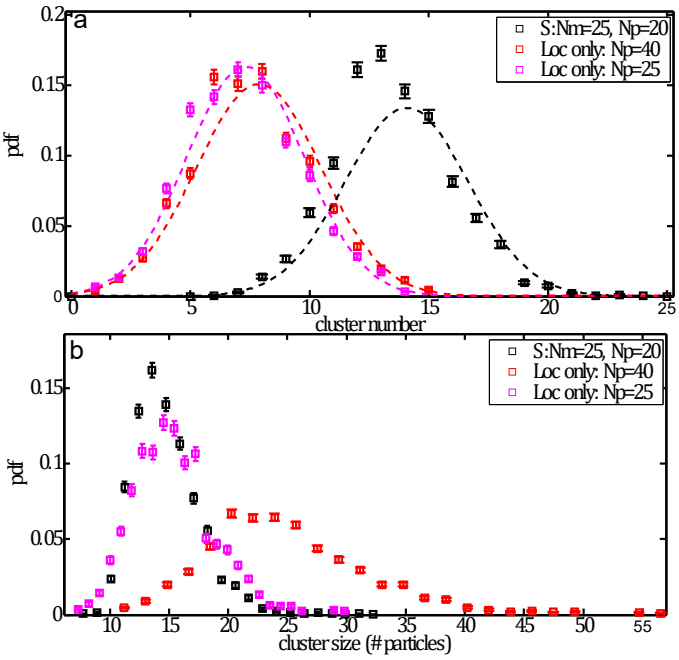

Fig. 5 a) The number of clusters for the standard soft spots algorithm (black), as well as when using only the localized augmented modes ($R_G < 16$), with $N_p = 25$ (magenta) and $N_p = 40$ (red). Using only the localized modes gives fewer spots. Dashed lines are Gaussian fits. b) The average number of particles per soft spot. Colors are same as in a) .